EPJ manuscript No.
(will be inserted by the editor)

Influence of plasma chemistry on oxygen triplets

V. Milosavljević[1,4], A. R. Ellingboe[2], and S. Daniels[3]

[1] NCPST & School of Physics, Dublin City University, Dublin 9, Ireland

[2] Plasma Research Lab, School of Physics & NCPST, Dublin City University, Dublin 9, Ireland

[3] NCPST & School of Electronic Engineering, Dublin City University, Dublin 9, Ireland

[4] Faculty of Physics, University of Belgrade, P.O. Box 368, Belgrade, Serbia

Received: 11 April 2011/ Revised version: 30 July 2011

Abstract. The plasma chemistry of fluorocarbon–oxygen–argon discharges and its influence on prominent oxygen triplets are studied. The oxygen 777 triplet is very important for the measurement of atomic oxygen in low pressure plasmas, since the 777.417 nm spectral line is frequently used for actinometry. In this paper we identify changes in the individual 777 triplet lines arising from cascade effects from higher energy levels of oxygen, and from resonant energy transfer from energetic carbon atoms in carbon-rich plasmas. The lower energy levels of three oxygen triplets (544 nm, 616 nm, 645 nm) are the upper states of the 777 triplet. Increased emission intensity from the 544, 616, and 645 triplets result in changes to the relative intensity of the individual lines of the 777 triplet, and this can lead to errors in using the 777 triplet, e.g. for actinometry. Also, in operational conditions with strong carbon emission (around 601 nm), the relative intensity of the individual oxygen 777 lines is affected. The upper energy levels of these carbon lines is close to the oxygen 777 upper energy levels, suggesting that resonant energy transfer between the carbon and the oxygen is occurring. The experiments are performed in a commercial semiconductor dielectric etcher operating with dual rf frequencies of 2 MHz and 27 MHz. Pressure (13-19 Pa), rf power (200-1200 W), and gas mixtures (argon with addmixtures of 5-13 % oxygen and C_4F_8) are typical in application to dielectric etching.

PACS. 32.70. Jz Line shapes, widths, and shifts – 52.25. Ya Neutrals in plasmas – 52. 70. -m Plasma diagnostic techniques and instrumentation

1 Introduction

Plasma deposition, etching, and surface modification are an integral part of modern technologies and pose many new challenges in the control of plasma chemistry. In contrast to the past, when mainly noble gas discharges were studied, the present interests are spread over a large variety of complex chemical systems.

In particular electronegative gas (like oxygen) plasmas attract much attention, in applications related to surface processing [1], at atmospheric pressure [2], environmental studies [3] for disposal gas cleaning and many others [4]. Oxygen plasmas have found numerous applications in plasma processing such as reactive sputtering, dry etching of polymers, oxidation, and resist removal in semiconductor manufacturing (ashing). Especially an oxygen plasma generated with RF discharges [5] has been found to be very effective for plasma etching, surface activation, cleaning, and oxidation of different materials.

Oxygen plasma is thermodynamically in a non–equilibrium gas phase, excited particles tend to de–excite, often by photon emission. Optical emission spectroscopy (OES) can be a powerful tool for plasma diagnostics [6, 7]. The emitted radiation intensity depends on the nature of the excited states. Radiation from metastable states, for instance, is usually not observed, while the strongest emission is often observed from atomic transitions. Oxygen atoms are formed in oxygen plasma primarily by two competing processes; electron impact dissociation and dissociative attachment. The density of excited atoms depends on the production and loss rates. While the production rate depends only on the electron temperature and density, the loss rate depends on numerous parameters, including the pressure, the characteristics of the discharge chamber, and the material properties of the plasma boundary.

Optical actinometry is an OES technique which is widely used for in–situ monitoring of spatial and temporal variations of atomic and molecular concentrations [8–11]. This technique uses the addition of a small amount of gas in the discharge e.g. noble gas where the intensities of its spectral lines are known to be representative of the excitation mechanism. To determinate the density of oxygen in the plasma, argon is frequently chosen as the actinometer gas because the transition $3s^2 3p^5 4s$–$3s^2 3p^5 4p$ from multiplet $^2[1/2]^o_1$–$^2[1/2]_0$ at 750.387 nm is insensitive to two step excitation [12]. The excitation of the $^2[1/2]_0$ 4p level in Ar I is 13.48 eV [13] which is higher than the excitation threshold for the $^4S^o$ 3p level in O I of 10.74 eV. A well known condition for actinometry is that the excited state of the actinometer (in this case argon) should have nearly the same energy as the excited state of the species of interest (i.e. oxygen). However there is a 2.7 eV difference between oxygen and argon electronic thresholds and thus it is clear that this condition is not satisfied. Nevertheless, if the remaining conditions for actinometry are fulfilled [14], then a difference between the energies of the excited states of argon and oxygen is not so critical and therefore Ar I 750.387 nm and O I 777.417 nm can be used for actinometry purposes [15, 16]. Comparison of the emitted line intensity for the desired species under examination (O,

Send offprint requests to: A. R. Ellingboe (be@physics.dcu.ie)

O_2) with the intensity of an emitted line of argon, allows one to eliminate the influence of line intensity changes due to excitation conditions and evaluate the real behavior of the emitted line intensity due to the changes in the species ground state concentration. The relative density of atomic oxygen can be monitored by calculating the ratio of the 3s–3p line intensity at 777.417 nm for O I and the 4s–4p line intensity at 750.387 nm for Ar.

Previous work [9] showed that the actinometric line from the 845-oxygen triplet is better suited than the 777-oxygen line. They show that the cross section for excitation by molecular dissociation is lower for the 845 line resulting in reduced signal masking. However, many spectrometers have very low quantum efficient for wavelengths of 800nm and above [17]. Therefore the oxygen 845 triplet can result in low signal intensity compared with the 777 oxygen spectral lines, and this can cause problems when developing applications based on actinometry. This fact is very important and often neglected in theoretical/practical comparison between the 777 and 845 oxygen triplets.

There are, however, other issues in the application of actinometry. For example, 777.417 nm atomic oxygen (O I) spectral line is part of an oxygen triplet, each has the same transition probability and many spectral devices cannot separate these spectral lines and therefore they record them as single line, i.e. "777" O I spectral line. In many technological plasma, also, a noble gas is a buffer gas and therefore the actinometric applications of the 777 spectral lines are even more challenging [18,19].

The conclusion of this work is that there are regions of operational space where the unresolved 777 oxygen line can be used as a substitute for the real oxygen actinometric line (777.417 nm) [20] but care must be taken. We demonstrate that the upper energy level of the 777 oxygen spectral lines can also be populated by cascade radiative emission from other oxygen triplets (e.g. 544, 616, and 645 O I triplets) and we establish the cascade dependency among those energy levels and external experimental conditions. Complexity of plasma chemistry is also investigated in this work, in particular the link between emission of several atomic carbon lines (600.113 nm, 600.603 nm, 600.718 nm, 601.068 nm, 601.322 nm and 601.484 nm) and the oxygen spectral lines from the 777 triplet. The upper energy levels among these spectral lines of oxygen and carbon are very close to each other, and we conclude that non–radiative transfer of energy between these carbon and oxygen energy levels occurs.

Our main motivation for this work is to (1) emphasize the influence of radiative emission from oxygen triplets at 544, 616, and 645 nm to the intensities of (one of most important) oxygen spectral lines at 777 nm, (2) present a non–radiative energy transfer between oxygen and carbon energy levels and the impact to spectral line emission of the 777 oxygen triplets, (3)study the influence and importance of quantum efficiency of the spectrometers to measurement of spectral intensity of the 777 "line", and (4) establish a criterion when it is suitable to use a low resolution spectrometer instead of a high resolution one for recording spectral lines at 777 nm.

2 Experimental setup & Diagnostics techniques

The experiments are performed in a modified Exelan® chamber (with Lam's proprietary DFC® technology). The experimental setup is shown schematically in Figure 1[21]. The topology of the plasma source is that of a parallel plate system with a 13 mm gap. The grounded upper electrode is made from a 6 mm thick single crystal silicon plate. The lower electrode consists of an electrostatic-chuck (ESC) which holds a 200 mm diameter silicon wafer with a 20 μm thermal oxide coating as the plasma facing boundary. The radial boundary of the plasma is formed by a set of quartz confinement rings. The net result of these boundary conditions is a symmetric plasma independent of the rf power and resultant plasma density.

The radio-frequency power delivered to the lower electrode of the system is a true summation of 2 MHz and 27 MHz signals (current and voltage). Typical values are 2 kV_{pp} (2.5 Amps) and 250 V_{pp} (25 Amps) for the 2 MHz and 27 MHz signals into the plasma, respectively. In combination with the symmetric plasma system, the plasma potential (V_p) oscillates predominantly at the 2 MHz rf voltage with an associated high frequency oscillation at 27 MHz [22,23], with the mean time–averaged V_p reaching several hundreds of volts above ground. The advantage of dual-rf-frequency power is that it provides independent control of the ion current and ion energy onto the boundary [24,25]. For the capacitive plasma configuration the high (low) frequency sees a low (high) impedance, resulting in high (low) current and low (high) voltage. The rf current results in ohmic heating of the plasma electrons, thus the high frequency power is principally responsible for power deposition into the electrons. The rf voltage on the electrode results in sheath voltage (the plasma bulk being highly conductive), thus the low frequency power is principally responsible for ion power delivered to the boundary and the ions gain the average sheath voltage when they cross the sheath. In this way dual-frequecy provides separate "control knobs" for ion current (proportional to density) and ion energy.

The gas is introduced into the chamber through a showerhead in the top (grounded) electrode. Gas flows through the plasma chamber radially and is pumped out between "confinement rings" into a pump channel which is connected to a helical–groove pump via a high–conductance pumping plenum. Constant plasma area pressure under varying reactive gas flows is achieved by varying the conductance of the confinement rings.

For the work presented here, the operating conditions involve a working gas containing a mixture of argon (Ar), oxygen (O_2), and cyclic–octafluorocyclobutane–RC318 (c -C_4F_8) in a flowing regime. The operating pressure of the plasma volume varies from 13 to 19 Pa (97 to 130 mTorr), while the corresponding Argon flow is constant all the time at 130 sccm. Gas flow of O_2 and C_4F_8 each range from 7 to 20 sccm, the gas flows being controlled by massflow controllers. Helium pressure of 1.33 kPa (10 Torr) is maintained on the backside of the wafer, resulting in a small (3-5 sccm) helium flow into the plasma volume. The RF

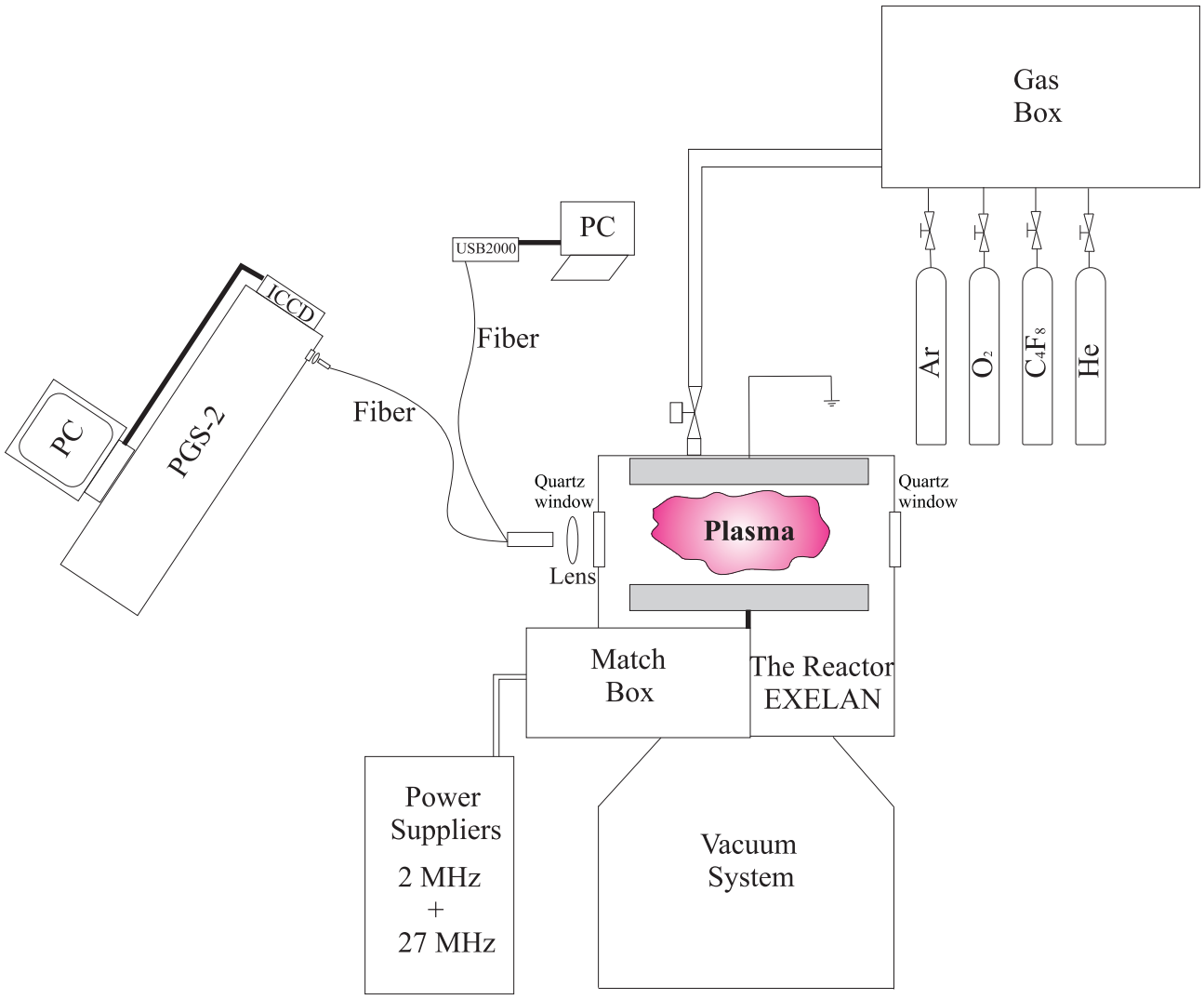

Fig. 1. Schematic diagram of the EXELAN chamber and associated diagnostics.

power of the lower frequency (2 MHz, $P2$) generator is varied from 200 to 600 W, and for the higher frequency (27 MHz, $P27$) generator the power is varied from 600 to 1200 W.

To collect OES data covering the multivariate process space (Oxygen flow, C_4F_8 flow, $P2$, $P27$, Pressure) and evaluate the cross-dependencies of the measured outputs, a "design-of-experiment" (DOE) approach has been taken. Eighteen different combinations of experimental parameters were selected to characterize the use of the oxygen-777 actinometry line. Details of the 18 operational points are given in table 1. To collect each emission spectra the system is sequentially operated in each of the 18 operational points, with dwell times at each point of 30 seconds. The sequence is run separately for data collection from each of the two spectrometers (described below). In this way long-time-scale chamber drift due to build-up and etching of the fluorocarbon films on the plasma boundaries that can occur for some operational points do not affect the data sets. Cleaning of the plasma-volume with a pure oxy-

Table 1. Process space DOE which approximates the operational region used in development of generic dielectric etch recipes.

Operating point	$P2$ 2 MHz power (Watts)	$P27$ 27 MHz power (Watts)	O_2 flow (sccm)	C_4F_8 flow (sccm)	Total Pressure (Pa)
1	600	1200	20	7	19
2	200	1200	20	7	13
3	600	600	20	20	19
4	600	1200	7	20	19
5	600	1200	7	7	13
6	600	600	7	20	13
7	200	600	7	7	13
8	600	1200	20	20	13
9	200	1200	7	20	13
10	200	1200	7	7	19
11	200	1200	7	7	13
12	200	1200	20	20	19
13	200	600	20	20	13
14	200	600	7	20	19
15	200	600	20	7	19
16	600	600	7	7	19
17	600	600	20	7	13
18	200	1200	7	7	19

gen plasma from time-to-time ensures a stable discharge condition.

All optical observations were carried out using one of two spectrometers. The first spectrometer is a 2 m focal length Carl Zeiss PGS-2 spectrometer with a 1302 lines/mm grating which operates from 200 to 1400 nm and has an ICCD camera system, which is sensitive from 190 nm to 900 nm, positioned at its focal plane. The PGS-2/iCCD optical system has very high resolution of 9.17 pm/pixel at λ=200 nm and 7.5 pm/pixel at λ=900 nm at the optimum entrance slit width of 15 μm. Although the PGS-2/iCCD optical system has very high resolution, it is bulky, difficult to operate and align and covers just 5 nm spectral region across the CCD detector at any one time. The second spectrometer is an Ocean Optics USB2000 fiber optic spectrometer which is a low resolution spectrometer with a focal length of 42 mm, a 600 lines/mm grating which operates from 200 to 875 nm. The resolution of the USB2000 is 0.555 nm/pixel at λ=200 nm and 0.536 nm/pixel at λ=875 nm [6]. This compact spectrometer is easy to operate with no optical alignment required and can display the entire spectrum from 200 to 875 nm at any one time.

Light from the plasma passes through the quartz confinement rings and through a large window in the side of the vacuum chamber. A 20 mm diameter lens collects light from a column across the diameter of the chamber and focuses onto a 200 μm multi-mode fiber. The other end of the 2m long fiber is selectively connected to either of the two spectrometers.

The intensity of each spectral peak is determined by calculating the area under the line of interest as summed over a spectral region from -2.5 full width half maximum (FWHM) step size up to +2.5 FWHM step size from the spectral line peak central position. If the spectral line is clearly isolated from other emission lines, then the inten-

sity summation is straightforward. However, if other lines exist in close proximity to the spectral line of interest, as is the case for the O I 777 nm triplet, then the intensity summation has to neglect the intrusive line and the summation was performed down to the background continuum that exists in that spectral region.

In order to compare recorded spectra from these two spectrometers, calibration of optical detection system, i.e. a calculation of they quantum efficiency, is performed. The intensity measured by a spectrometer [17], depended on wavelength (λ), is given by

$$I_{\lambda}^{\mathrm{Spec}} = I_{\lambda}^{\mathrm{Sour}} \cdot \Omega_{\mathrm{eff}} \cdot \Delta A \cdot \Delta\lambda \cdot T_{\mathrm{F}} \frac{\lambda}{h \cdot c} \cdot T_{\mathrm{W}} \cdot Q_{\lambda}. \quad (1)$$

where $I_{\lambda}^{\mathrm{Sour}}$ is intensity of the light source depended of the wavelength, Ω_{eff} is the effective spatial angle, ΔA is the effective area of the source, $\Delta\lambda$ is the spectral interval, T_F is the transparency of the interference filter, T_W is the transparency of the window on light source and Q_λ is the quantum efficiency of Spectrometer. Figure 2 shows the normalized quantum efficiency of the two spectrometer systems.

There are 21 energy levels [13] from the spectrum of O I with transitions to the 3p (^{5}P) level is allowed and some of those are presented in Figure 5 and Table 2. As presented in Table 2, five of the 21 possible O I energy levels exhibit high transition probability to the 3p (^{5}P) levels. From the 6s ($^5S_2^o$) energy level three transition to the 3p level are possible. The wavelengths of these three spectral lines are very close to each other and are called the atomic oxygen 544 triplet. From the 5s ($^5S_2^o$) energy level there are three transition to the 3p level, and these transitions belong to the atomic oxygen 645 triplet. The 4d multiplet ($^5D^o$) exhibit energy splitting due to the different inner quantum number, resulting in the compound oxygen 616 triplet. Eight other oxygen spectral lines with upper energy levels (3d $^5D^o$) of about 12.0786 eV [13] and lower energy level is the 3p (^{5}P) may impact emission of the spectral lines to the 777 oxygen triplet. Unfortunately, wavelengths of these eight O I spectral lines are at approximately 926 nm and our spectrometer can not observe them. Therefore, we have focused our study on the spectral lines from 543, 616 and 645 triplets. The difference in the intensity of the spectral lines from the 777 oxygen triplet can be explained by differences in transition probabilities of the spectral lines from 544, 616 and 645 oxygen triplets. Namely, all spectral lines from the 777 triplets have the same transition probabilities, but the individual spectral lines from each of the 544, 616 and 645 triplets have different transition probabilities. The maximum transition probably in the 544 multiplet has spectral line of 543.686 nm and the minimum has spectral line of 543.518 nm. For the oxygen 616 triplet, the maximum transition probability has spectral line of 615.819 nm and the minimum has spectral line of 615.667 nm. In the case of the 645 triplet, the maximum transition probability has spectral line of 645.598 nm and the minimum has spectral line of 645.360 nm (see Table 2). Other transitions exist with lower energy of 3p (^{5}P), but with substantially lower transitions probabilities and measured intensities, and the impact of these is assumed to be small.

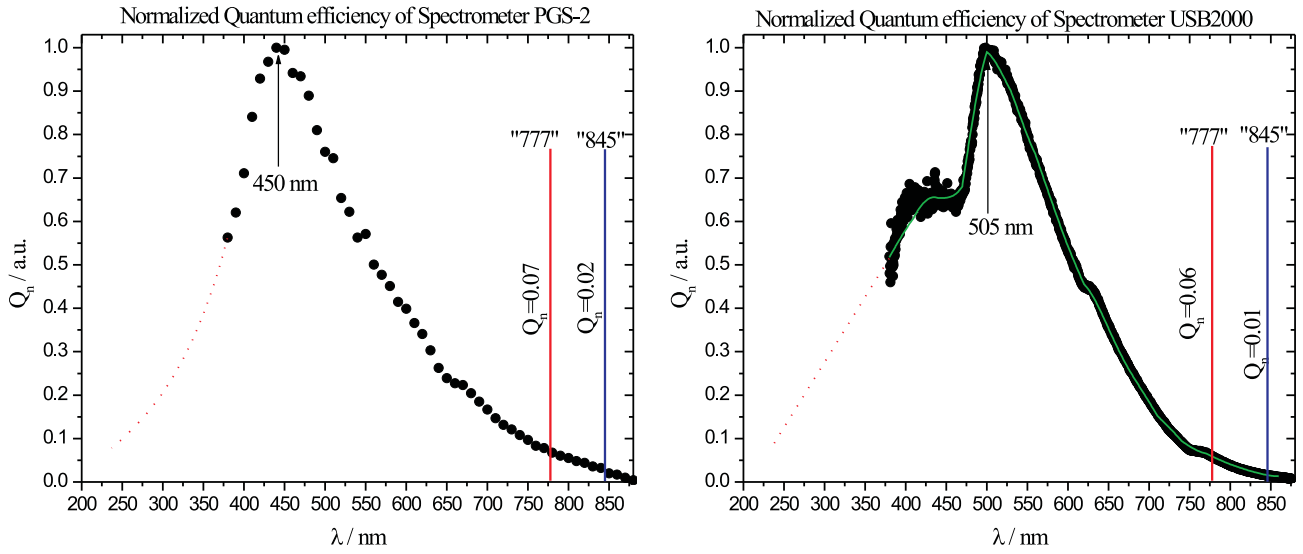

Fig. 2. The normalized quantum efficiency calculated by equation 1 for the PGS-2 (left) and the USB-2000 (right).

Atomic oxygen has two actinometry spectral lines, the first one belongs to the 777 triplet and the second one belongs to the 845 triplet. Figure 2 shows that both spectrometers have very low efficiency at a wavelength of 845 nm (vertical line with label "845"). The quantum efficiency is much higher at 777 nm (vertical line with label "777") than for 845 nm, i.e. 3.5 times is higher in the high resolution spectrometer and 6 times for the low resolution spectrometer. This leads to the conclusion that many spectrometers will record very low signal intensity of the 845 oxygen triplet, and this is a problem for actinometry. This is not the only problem with recording the 845 oxygen triplet. Namely, for actinometrical purpose it is necessary to add a small amount of actinometry gas, e.g. argon. Argon has very strong spectral line emission between 700 and 850 nm, such that even small amounts of argon will introduced significant radiative emission. Figure 3 shows the spectra from a pure oxygen plasma with an overlay of the spectra from a pure argon discharge. The deconvolution between the 845 and the 842.4 nm spectral lines can be very challenging. According to the NIST database, the lines from 845 multiplet have about 20% higher relative intensity than the 777 multiplet, see Table 2. However, the measured intensity of spectral lines (figure 3) from the 777 multiplet is higher than the 845 multiplet due to quantum efficiency of these spectrometers (about four times in average). Therefore, it is worth exploring the option to use the spectral line from the 777 triplet for oxygen actinometry.

3 Results and Discussion

The 777 nm oxygen triplet includes three spectral lines, see Table 2. These lines belong to transition 3s–3p and multiplet $^5S^o$–^5P. They have the same lower energy (E_f) level of 9.15 eV, while the upper energy (E_i) levels are

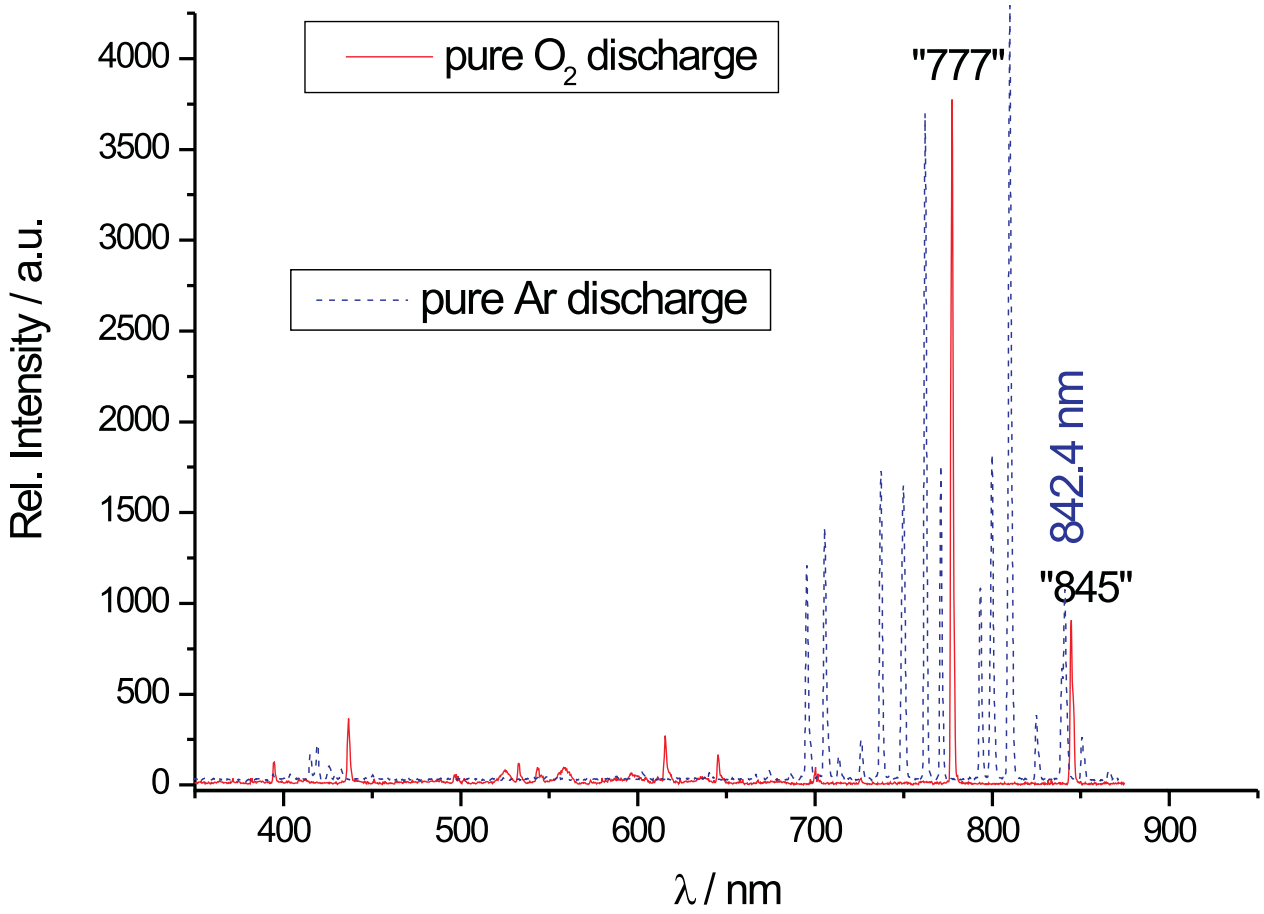

Fig. 3. Typical optical spectrum of pure oxygen discharge (solid line) and pure argon discharge (broken line) recorded by the USB2000 spectrometer.

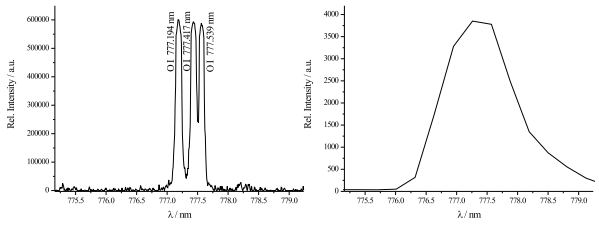

Fig. 4. O I "777" spectral lines recorded by the PGS-2 spectrometer (left) and by the USB2000 spectrometer (right) at operation point number 1 (see table 1)

very close to 10.740 eV (energy spread is 0.0007 eV) Due to the limited resolution of most available spectrometers, this triplet is often recorded as a single spectral line (figure 4, right).

Three other oxygen triplets are the 544 (543.686 nm, 543.578 nm and 543.518 nm), 616 (615.818 nm, 615.677 nm and 615.598 nm) and the 645 (645.598 nm, 645.444 nm and 645.360 nm). The lines from 544, 616 and 645

Table 2. Spectroscopic data of the relevant emission spectral lines. The transition probability values (A), wavelengths, transitions, initial energy levels (E_i) and final energy levels (E_f), are taken from reference [13].

Emitter	λ (nm)	Transition	Multiplet	Rel. Intensity (a.u.)	A (1/s)	E_i (eV)	E_f (eV)
O I	777.194	3s–3p	$^5S^o_2$–$^5P_3$	870	3.69 10^7	10.740931	9.1460906
	777.417	3s–3p	$^5S^o_2$–$^5P_2$	810	3.69 10^7	10.740475	9.1460906
	777.534	3s–3p	$^5S^o_2$–$^5P_1$	750	3.69 10^7	10.740224	9.1460906
	844.625	3s–3p	$^3S^o_1$–$^3P_0$	810	3.22 10^7	10.988880	9.5213632
	844.636	3s–3p	$^3S^o_1$–$^3P_2$	1000	3.22 10^7	10.988861	9.5213632
	844.676	3s–3p	$^3S^o_1$–$^3P_1$	935	3.22 10^7	10.988792	9.5213632
	543.518	3p–6s	$^5P_1$–$^5S^o_2$	90	7.74 10^5	13.0207338	10.740224
	543.578	3p–6s	$^5P_2$–$^5S^o_2$	110	1.29 10^6	13.0207338	10.740475
	543.686	3p–6s	$^5P_3$–$^5S^o_2$	135	1.80 10^6	13.0207338	10.740931
	645.360	3p–5s	$^5P_1$–$^5S^o_2$	320	1.65 10^6	12.6608561	10.740224
	645.444	3p–5s	$^5P_2$–$^5S^o_2$	360	2.75 10^6	12.6608561	10.740475
	645.598	3p–5s	$^5P_3$–$^5S^o_2$	400	3.85 10^6	12.6608561	10.740931
	615.598	3p–4d	$^5P_1$–$^5D^o_1$	400	5.72 10^6	12.7537150	10.740224
	615.677	3p–4d	$^5P_2$–$^5D^o_3$	450	5.08 10^6	12.7537016	10.740475
	615.818	3p–4d	$^5P_3$–$^5D^o_4$	490	7.62 10^6	12.7536965	10.740931
C I	600.113	3p–6s	$^3D_2$–$^3P^o_2$	200	3.22 10^5	10.70846	8.643020
	600.603	3p–5d	$^3D_3$–$^3D^o_2$	250	3.14 10^4	10.71092	8.647157
	600.718	3p–6s	$^3D_1$–$^3P^o_1$	110	5.34 10^5	10.70376	8.640394
	601.068	3p–6s	$^3D_1$–$^3P^o_0$	150	2.13 10^6	10.70256	8.640394
	601.322	3p–5d	$^3D_3$–$^3F^o_4$	300	4.35 10^5	10.70845	8.647157
	601.484	3p–6s	$^3D_2$–$^3P^o_1$	250	1.60 10^6	10.70376	8.643020

triplets have different E_i levels see Table 2. The E_f levels for spectral lines from the 544, 616, and 645 triplets are the E_i levels for spectral lines from the 777 triplet. The energy levels and associated spectra lines are presented in figure 5 and Table 2. We investigate the impact of 544, the 616 and the 645 triplet emission on the intensity of the 777 triplet lines.

The energy level of the upper state of the O-777 triplet is quite close to the energy levels of upper states of atomic carbon which give rise to emission at 601 nm. By monitor-

ing the 601 nm emission across the different operational conditions, the potential for disturbing the relative intensities of the O-777 triplet due to non-radiative energy transfer with atomic carbon is evaluated. The atomic carbon energy levels and transitions are presented in Figure 5 and Table 2.

The normalized relative intensity of oxygen spectral lines within its multiplet (figure 5) is proportional as well to transition probabilities of those lines. For example for oxygen lines from the 645 triplet, the relative intensity of the 645.360, 645.444 nm line, and the 645.598 nm lines are, respectively, 1.0:1.13:1.25, see Table 2 and figure 5. Since the different oxygen lines of the different triplets have different lower energy levels (i.e. upper energy levels of "777" lines), it can be expected that the oxygen spectral line intensities from 777 multiplet will not always be equal.

Figure 6 plots the intensity of the individual 777 triplet lines versus the operation points (see table 1). The top graph shows the line intensities; the bottom graph shows intensities normalized to the average at that operational point. As shown in Figure 6, the intensity of each line of the triplet around 777 nm in O I measured with the PGS-2 spectrometer exhibits similar behavior with changing rf power/pressure/gas-mixture for most plasma operating conditions tested here (table 1). This infers that although the actual actinometry spectral line is not resolved by the USB2000 spectrometer, the measured broad peak intensity can by multiplied by a certain factor to give the actual intensity of the actinometric emission line within the particular unresolved peak. This is true for the majority of the operating conditions but not for all of them. For example, figure 6 shows significant difference between the oxygen 777 spectral lines for operation points: 3, 8, 9, 14, 15, and 16. Common among operation conditions 3, 14, 15, and 16 are minimum $P27$ power and maximum pressure. In these conditions the individual O777 intensities spread, thus in addition to the main mechanism for population of 3p ($^5P_{1,2,3}$) by electron impact excitation from ground state, other optical channels must play an important role.

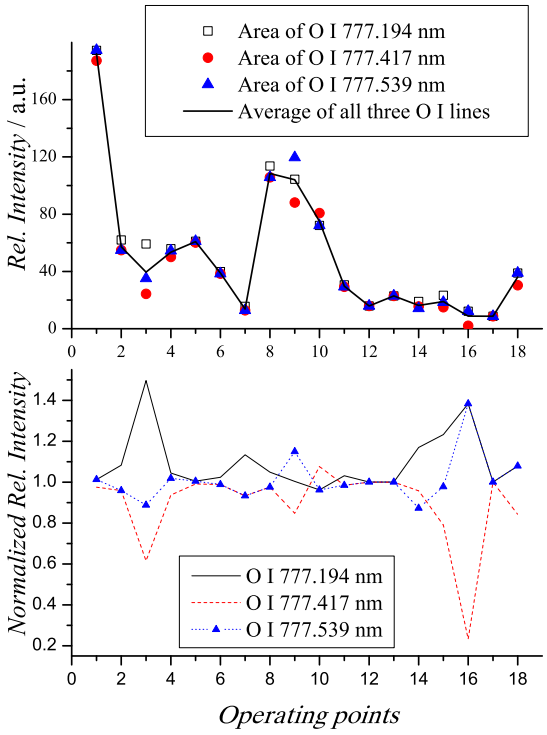

Fig. 6. The Intensities of atomic oxygen spectral lines from the 777 multiplet measured by PGS-2 spectrometer vs. operating points.

Figure 7 gives the normalized intensity of each oxygen spectral lines from the 777 triplet versus the relative inten-

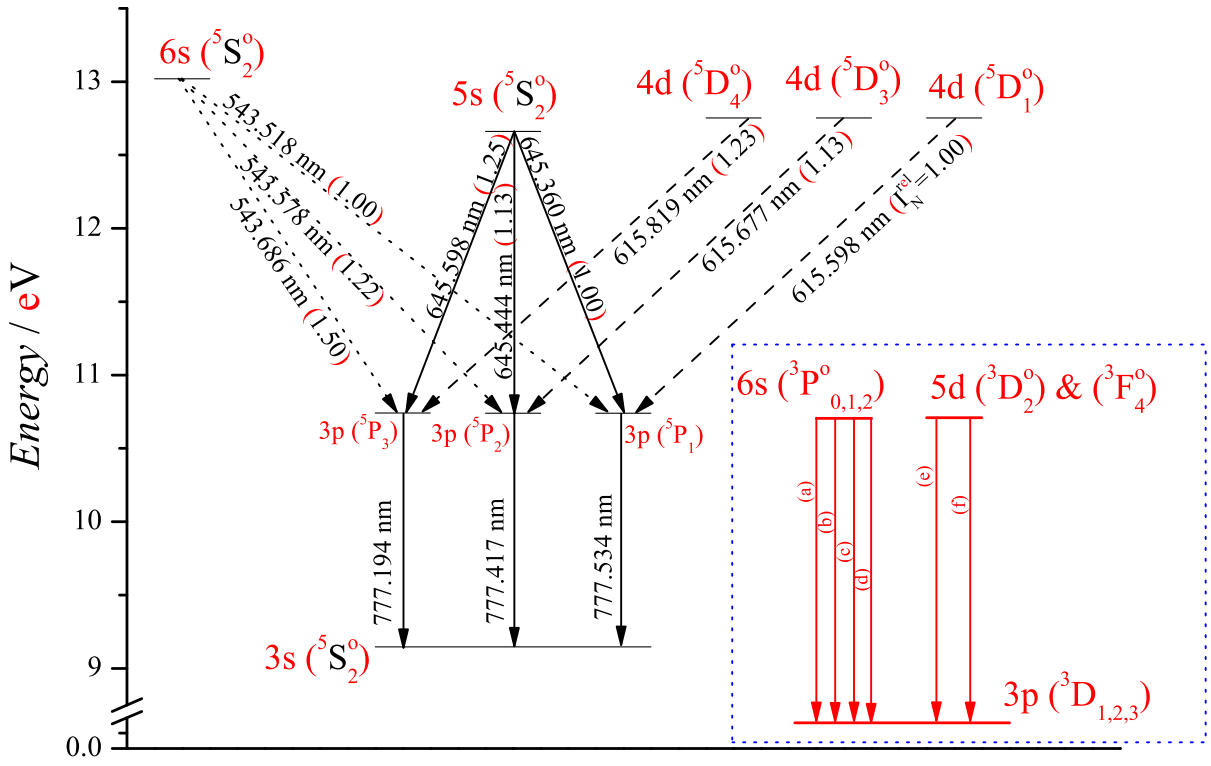

Fig. 5. Atomic oxygen and carbon spectral lines with upper and lower energy levels. In the bracket next to the oxygen wavelengths are normalized intensity of the spectral lines within its multiplet. In the dotted square are spectral lines from atomic carbon spectrum, small caps in the bracket represents the following spectral lines: (a) 600.113 nm, (b) 600.718 nm, (c) 601.068 nm, (d) 601.484 nm, (e) 600.603 nm, and (f) 601.322 nm.

sity of the other three oxygen triplets. Figure 7 top plots versus the 544 intensity, middle versus 616 intensity, and bottom versus 645 intensity. Common to all three graphs are very low intensity (x-axis) of the oxygen spectral lines from 544, 616 and 645 triplets for the majority of operating conditions. At these same conditions there is very low scatter of intensity (y-axis) for spectral lines from the 777 oxygen triplet. In contrast, for the operation points 3, 14, 15, and 16, all spectral lines from the 544, 645, and 616 triplets have very high relative intensity (about an order of magnitude higher then for other operation points). For these 4 operating points, the spectral lines from the 777 triplet have very high scatter of intensities. This gives strong evidence of cascade effects from the 544, 616, and 645 triplets on the relative emission intensities of the 777 triplet.

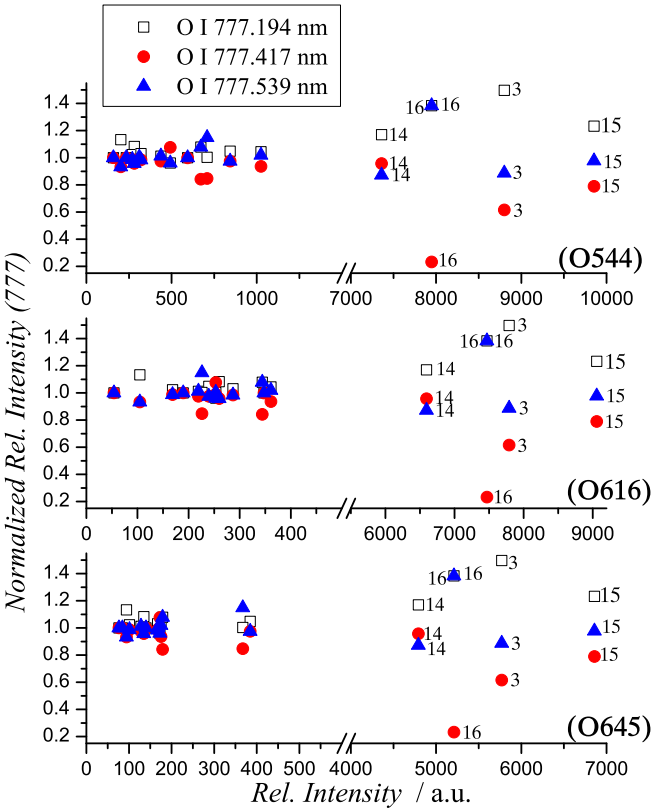

Fig. 7. Distribution of the normalized intensity of the oxygen spectral lines from the 777 multiplet versus the intensity of the other three oxygen multiplets (in the brackets). The number next to symbols represents the operation points from table 1.

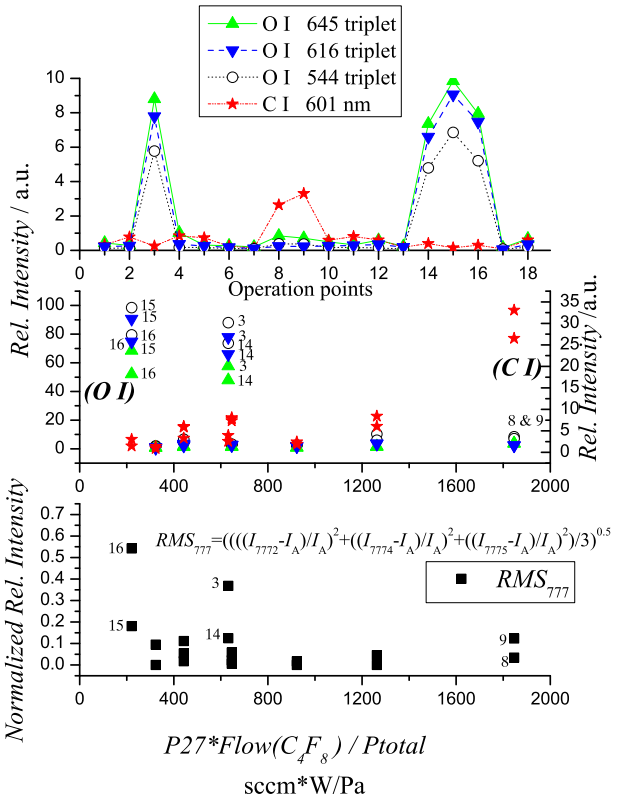

Fig. 8. Top: Atomic oxygen and carbon spectral lines vs. the operation points (see table 1). Middle: Atomic oxygen and carbon spectral lines vs. a compound x-axis, see text. Bottom: The root mean square normalized intensity of the 777 oxygen triplet vs. a compound x-axis, see text. The number next to symbols represents the operation points from the table 1.

Figure 8 (top) presents measured intensities of the spectral lines from 544, 616 and 645 triplets and Carbon emission at 601 nm versus the operational point (see table 1). The recorded radiative emission of the spectral lines from the 544, 616, and 645 triplets are significant only for the operation points 3, 14, 15 and 16. The emissions of the spectral lines for these three triplets are small for the other 14 operation points. Emission at 601 nm from atomic carbon is large at operational points 8 and 9.

To understand the phenomenology of the oxygen triplets, note that at the conditions where the 544, 616, and 645 emission is high (operational points 3, 14, 15, and 16), the P27 is at a minimum value and total pressure is at a maximum, thus the ratio of high frequency power to pressure is a minimum. In these conditions, we observe that the population of 3p level ($^5P_{1,2,3}$) by electron collision from ground state is no longer the main/only mechanism. Other optical channels play an important role as well, e.g.

the cascade population of the 3p level by radiative transfer from high lying energy levels. This additional mechanism results in scatter in the O777 triplet line intensities for these conditions. The deviation in intensity of the spectral lines from the 777 multiplet occurs when the intensities of the 544, 616 and 645 multiplets show large increase in intensity. This is presented in figures 7 and 8 (top and middle graphs). One possible mechanism is molecular dissociation pathways leading to highly excited states of atomic oxygen. The energy threshold for the molecular dissociation pathway is much higher than for excitation directly from the ground-state atomic oxygen [9].

The relative increase in emission from the high-energy pathways (cascade from higher energy states, in particular following molecular dissociation) at the low P27 conditions can be understood by the following argument based on global model of the discharge. Low P27 results in low plasma density. This, in turn, results in higher 2 MHz voltage. The combination of low density and high voltage results in larger sheath width. For our chamber geometry with only 12 mm separation between the electrodes, the sheath expansion causes a significant decrease in the plasma characteristic length, $l = d - 2s$ where d is the electrode separation and s is the maximum sheath-extent [25]. As sheath extents have been measured to be several millimeters [22] the change in plasma extent can be quite significant. Global model requires (on average) each electron-ion pair to have an ionization event before it is lost. Thus the electron temperature will increase as the sheath width increases and plasma length decreases. There are two further effects which could increase the high-energy population of the electron distribution function. First, increased sheath voltage will increase the energy of secondary electrons. Second, the increased sheath extent will result in a higher velocity sheath edge. The effect of the dual-frequency sheath resulting in the formation of energetic beams phase-locked to the expansion phase of the dual-frequency sheath has been experimentally observed [26]. Theses 'beams' have energies greater than the threshold for molecular dissociation into the upper states of atomic oxygen leading to the cascade population of the oxygen triplets. These three effects all favor (relatively) the formation of high energy states which include both the dissociative pathways mentioned above and the direct excitation of the high-energy states of oxygen from the ground state.

To understand the impact of atomic Carbon on the oxygen 777 emission lines note that for operation points 8 and 9 (the two points with high intensity carbon line emission, Fig 8 top) $P27$ is at a maximum, the total pressure is the minimum, and the flow of C_4F_8 is the maximum. That is, high power density per gas molecule and high fractional carbon content. It is not surprising that this combination results in the highest measured atomic carbon emission intensities. The 601 nm C I line consists of six discrete lines (600.113 nm, 600.603 nm, 600.718 nm, 601.068 nm, 601.322 nm and 601.484 nm). The upper energy levels associated with these lines are very close (about 0.02 eV) to the energy of 3p oxygen level (see Figure 5 and Table 2).

Figure 8, middle, re–plots the same emission intensities but now versus the product of the $P27$, C_4F_8 flow, and inverse of pressure. The left Y-axis represents the intensity of oxygen spectral lines and the right Y-axis represents the intensity of carbon spectral lines. The X-axis is common for both Y-axis with physical interpretation as described above. As mentioned previously, the emission of oxygen spectral lines from from 544, 616 and 645 triplets are very low for majority of the operation points. Those values stay at order of magnitude less then for operation points of 3, 14, 15, and 16. At operational points 8 and 9, the same graph gives evidence of coupling between the carbon spectral lines emission and spectral emission of the oxygen spectral lines from the 777 multiplet. Namely, the emission of spectral lines within the 777 oxygen triplet significantly scatter from average value (see figure 6) for the operating points 8 and 9, at the same conditions where the carbon spectral lines emission intensity is high and O-544, O-616, and O-645 triplet emission intensities are low. In a plasma the most efficient process are an resonant one and in collisions between oxygen and carbon atoms there is the possibility of non–radiative transfer of an energy. This leads to the conclusion that the atomic carbon is interfering with the O-777 line strengths.

The last graph, in the bottom on figure 8 is dependence between the root mean square (RMS) of the normalized intensity for the 777 oxygen triplet and the same compound X-axis. In the formula on the top of this graph, I_A is the average intensity of the 777 triplet, and the indexes 7772, 7774 and 7775 are the individual spectral lines of the 777 triplet. Otherwise, the RMS also known as the quadratic mean, is a statistical measure of the magnitude of a varying quantity. From this graph is clear that for the 6 operation points (3, 8, 9, 14, 15, and 16) spectral emission of the 777 oxygen spectral lines it not dependent only on the electron collision from ground state.

4 Conclusions

Optical emission spectroscopy was used to study the characteristics of the oxygen actinometry spectral line (777.417 nm) in fluorocarbon–oxygen–argon plasma, created by dual–frequency RF discharge. The intensity of select atomic oxygen and carbon spectral lines have been monitored for various operation points across a multi-variate parameter space.

For many operating conditions the dominant mechanism for populating the upper state (^3P) of the O-777 triplet is electron collision from the ground state, and thus it is valid to use the 777.417 nm line in actinometry. Furthermore, in these cases the three emission lines from the O-777 triplet have nearly equal intensity and the unresolved O-777 triplet can be used as the actinometer.

However, for some operational cases the upper state of the O-777 line is populated through other mechanisms as well, and neither the O-777 triplet line nor the 777.417 nm actinometer line within the triplet are valid. High resolution spectroscopy resolving the O-777 triplet in addition to monitoring select other high emission intensity lines (Oxygen 544, 616, and 645 triplets and atomic carbon 601 multiplet) in a dual-frequency confined capacitively-coupled

plasma (DFC-CCP) has identified two mechanisms that interfere with using the O-777 line for actinometry. The first correlates to strong cascade emission from higher-energy states of atomic oxygen, and this supports previous work [9]. In the DFC-CCP this occurs at low $P27$ and is understood to be due to increase in the electron temperature and/or preferential heating of the tail population of the electron-energy-distribution function. The second mechanism observed correlates to high atomic carbon emission. This is understood to be due to resonant energy transfer between the upper state of the O-777 lines (^3P state) and the ^6S and ^5D states of atomic carbon, since the resonance process have high probability.

Complex plasma chemistry can cause the low resolution 777 actinometer to fail. In particular, a strong correlation among intensity of lines from the 777 multiplet and 544, 616 and 645 triplets have been established. The plasma chemistry plays important role in the relative radiative emission of the 777 multiplet via cascade effects. Evidence is also seen for non–radiative energy transfer between carbon and oxygen atoms.

Acknowledgment

This work is a part of the fellowship award funded by SFI Precision project, and "VHF/UHF plasma source technology" funded by Enterprise Ireland. V. Milosavljević is grateful to the Ministry of Science and Technological Development of the Republic of Serbia under grant No. OI171006.

References

1. K. von Haeften, C. Binns, A. Brewer, O. Crisan, P.B. Howes, M.P. Lowe, C. Sibbley–Allen, S.C. Thornton, A novel approach towards the production of luminescent silicon nanoparticles: sputtering, gas aggregation and co–deposition with H_2O, Eur. Phys. J. D **52**, 11-14 (2009).
2. J. Schäfer, R. Foest, A. Quade, A. Ohl, J. Meichsner, K. D. Weltmann, Carbon–free SiO_x films deposited from octamethylcyclotetrasiloxane (OMCTS) by an atmospheric pressure plasma jet (APPJ), Eur. Phys. J. D **54**, 211-217 (2009).
3. Z. Machala, I. Jedlovský, L. Chládeková, B. Pongrác, D. Giertl, M. Janda, L. Šikurová, P. Polčic, DC discharges in atmospheric air for bio–decontamination spectroscopic methods for mechanism identification, Eur. Phys. J. D **54**, 195-204 (2009).
4. S. Gilb, K. Hartl, A. Kartouzian, J. Peter, U. Heiz, H.-G. Boyen, P. Ziemann, Cavity ring–down spectroscopy of metallic gold nanoparticles, Eur. Phys. J. D **45**, 501506 (2007).
5. E. Grimoldi, S. Zanini, R.A. Siliprandi, C. Riccardi, AFM and contact angle investigation of growth and structure of pp–HMDSO thin films, Eur. Phys. J. D **54**, 165172 (2009).
6. V. Milosavljević, V. Žigman, S. Djeniže, Stark width and shift of the neutral argon 425.9 nm spectral line, Spectrochimica Acta Part B: Atomic Spectroscopy **59/9** (2004) 1423-1429.
7. V. Milosavljević, A. R. Ellingboe, S. Djeniže, Measured Stark widths and shifts of the neutral argon spectral lines in 4s–4p and 4s–4p' transitions, Spectrochimica Acta Part B: Atomic Spectroscopy **61/1** (2006) 81-87.

8. J. W. Coburn, M. Chen, Optical emission spectroscopy of reactive plasmas: A method for correlating emission intensities to reactive particle density, J. Appl. Phys. **51** (1980) 3134-3136.

9. R. E. Walkup, K. L. Saenger, G. S. Selwyn, J. Chem. Phys. **84/5** (1986) 2668.

10. S. De Benedictis, A. Gicquel, F. Cramarossa, Proc. 8th Int. Symp. Plasma Chem. ISPC'87, (Ed. K. Akashi, A. Kinbara), Tokyo (1987).

11. P. Macko, P. Veis, G. Cernogora, Study of oxygen atom recombination on a Pyrex surface at different wall temperatures by means of time–resolved actinometry in a double pulse discharge technique, Plasma Sources Sci. Technol. **13** (2004) 251-262.

12. T. Czerwiec, F. Greer, D. B. Graves, Nitrogen dissociation in a low pressure cylindrical ICP discharge studied by actinometry and mass spectrometry, J. Phys. D: Appl. Phys. **38/24** (2005) 4278-4289.

13. NIST – Atomic Spectra Data Base Lines (wavelength order) 2011 – http://physics.nist.gov

14. M. Lieberman, A. Lichtenberg, "Principles of Plasma Discharges and Materials Processing" (New York: Wiley), (1994).

15. S. Fujimura, K. Shinagawa, M. Nakamura, H. Yano, Additive Nitrogen Effects on Oxygen Plasma Downstream Ashing, Jpn. J. Appl. Phys. **29/10** (1990) 2165-2170.

16. A. Granier, D. Chéreau, K. Henda, R. Safari, P. Leprince, Validity of actinometry to monitor oxygen atom concentration in microwave discharges created by surface wave in O_2–N_2 mixtures, J. Appl. Phys. **75/1** (1994) 104-114.

17. V. Milosavljević, PRL Internal report, Dublin City University, Dublin (2004).

18. V. Milosavljević, R. Faulkner, M. B. Hopkins, Real time sensor for monitoring Oxygen in radio–frequency plasma applications, Optics Express **15/21** (2007) 13913.

19. D. Popović, V. Milosavljević and S. Daniels, Practical sensor for nitrogen in direct current glow discharges, Journal of Applied Physics **102** (2007) 103303.

20. H. Nagai, M. Hiramatsu, M. Hori, and T. Goto, Measurement of oxygen atom density employing vacuum ultraviolet absorption spectroscopy with microdischarge hollow cathode lamp, Rev. of Scien. Instr. **74/7**, (2003) 3453–3459

21. V. Milosavljević, A. R. Ellingboe, C. Gaman and J. Ringwood, Real–time Plasma controlled chemistry in a two–frequency, confined plasma etcher, Journal of Applied Physics **103/7** (2008) 083302.

22. S. K. Karkari, A.R. Ellingboe, C. Gaman, Appl. Phys. Lett. **93**, (2008) 071501

23. J. Robiche, P. C. Boyle, M. M. Turner, A. R. Ellingboe, J. Phys. D **36** (2003) 1810.

24. S. K. Karkari, A. R. Ellingboe, Appl. Phys. Lett. **88** (2006) 101501.

25. P.C. Boyle, A.R. Ellingboe, M.M. Turner, J. Phys. D: Appl. Phys. **37** (2004) 697–701

26. J. Schulze, T. Gans, D. O'Connell, U. Czarnetzki, A. R. Ellingboe, and M. M. Turner, J. Phys. D: Appl. Phys. 40 (2007) 7008–7018